Summer 2014

A small-scale experiment using microwave interferometry to investigate detonation and shock-to-detonation transition in pressed TATB

Peter John Renslow
Purdue University

Graduate School ETD Form 9
(Revised 01/14)

PURDUE UNIVERSITY
GRADUATE SCHOOL
Thesis/Dissertation Acceptance

This is to certify that the thesis/dissertation prepared

By Peter John Renslow

Entitled
A SMALL-SCALE EXPERIMENT USING MICROWAVE INTERFEROMETRY TO INVESTIGATE DETONATION AND SHOCK-TO-DETONATION TRANSITION IN PRESSED TATB

For the degree of Master of Science in Aeronautics and Astronautics

Is approved by the final examining committee:

Dr. Steven F. Son

Dr. Lori Groven

Dr. Stephan Beaudoin

Dr. Wayne Chen

To the best of my knowledge and as understood by the student in the *Thesis/Dissertation Agreement. Publication Delay, and Certification/Disclaimer (Graduate School Form 32)*, this thesis/dissertation adheres to the provisions of Purdue University's "Policy on Integrity in Research" and the use of copyrighted material.

Dr. Steven F. Son

Approved by Major Professor(s): _____

Approved by: Dr. Wayne Chen 05/15/2014

Head of the Department Graduate Program Date

A SMALL-SCALE EXPERIMENT USING MICROWAVE INTERFEROMETRY TO INVESTIGATE DETONATION AND SHOCK-TO-DETONATION TRANSITION IN PRESSED TATB

A Thesis

Submitted to the Faculty

of

Purdue University

by

Peter John Renslow

In Partial Fulfillment of the

Requirements for the Degree

of

Master of Science in Aeronautics and Astronautics

August 2014

Purdue University

West Lafayette, Indiana

ACKNOWLEDGEMENTS

First, I would like to thank Sandia National Laboratories and my manager Michael Hessheimer for the opportunity and funding to pursue a Master's degree in engineering. Second, thank you to the Department of Homeland Security and the ALERT Center of Excellence under Award 2013-ST061-ED0001 for their continued support on this research project. Third, I would like to thank my advisor Dr. Steven Son, as well as research faculty Dr. Lori Groven, Dr. Emre Gunduz, and Ph.D candidate David Kittell for their guidance and shared expertise. And last, thank you to my parents Pete and Cheryl Renslow for their continued support through my education and beginning of my career.

TABLE OF CONTENTS

LIST OF TABLES

Table Page

LIST OF FIGURES

Figure Page

ABSTRACT

Renslow, Peter J. M.S.A.A., Purdue University, August 2014. Small-Scale Experiment using Microwave Interferometry to Investigate Shock Initiation, Failure, and Transient Reactive Waves in Pressed TATB. Major Professor: Steven F. Son, School of Aeronautics and Astronautics (by courtesy).

A small-scale characterization test utilizing microwave interferometry was developed to dynamically measure detonation and run to detonation distance in explosives. The technique was demonstrated by conducting two experimental series on the well-characterized explosive triaminotrinitrobenzene (TATB). In the first experiment series, the detonation velocity was observed at varying porosity. The velocity during TATB detonation matched well with predictions made using CHEETAH and an empirical relation from the Los Alamos National Laboratory (LANL). The microwave interferometer also captured unsteady propagation of the reaction when a low density charge was near the failure diameter. In the second experiment series, Pop-plots were produced using data obtained from shock initiation of the TATB through a polymethyl methacrylate (PMMA) attenuator. The results compared well to wedge test data from LANL despite the microwave interferometer test being of substantially smaller scale. The results showed the test method is attractive for rapid characterization of new and improvised explosive materials.

CHAPTER 1. INTRODUCTION AND BACKGROUND

1.1 Introduction

The development of new energetic materials and ever-present threats from improvised or homemade explosives highlights the need for improving explosive characterization methods. Conventional explosive characterization tests – such as the wedge test and cylinder test – require relatively large quantities of explosive material, increasing costs and safety concerns. The resources necessary to fully characterize standard materials used in production capacity for mining and defense are available, but homemade and improvised threats present a unique challenge; homemade and improvised formulations are numerous, difficult to replicate, and constantly evolving. Therefore, the study of these materials at laboratory-scale adds significant benefit to characterization and modeling efforts by reducing costs and increasing safety.

The objective of this work was to dynamically measure detonation and shock-to-detonation transition with minimum explosive material in a small-scale experiment. To achieve this goal, a microwave interferometer (MI) was used to track the position of a shock wave through an explosive charge. The well-characterized explosive triaminotrinitrobenzene (TATB) was used to develop and demonstrate the accuracy of the experimental technique. TATB was chosen because of its performance, insensitivity, and it has been extensively studied in the literature. Data from the MI was compared to data from the simulation code CHEETAH and experimental data

from larger scale experiments. The goal was to demonstrate the usefulness of the experiment as a small-scale characterization tool for both new and established high explosives, including improvised and homemade materials.

1.2 Explosive Characterization Experiments

To determine performance characteristics such as run distance to detonation, accelerating ability, and corner-turning ability, common tests include the aforementioned wedge test, the cylinder test, corner-turning tests, and the particle velocity gauge technique. Traditional cylinder tests involve detonating an explosive charge in a copper sleeve and measuring the acceleration of the expanding copper to determine the energy in the explosive products [1, 2]. Data from these tests can be used in modelling applications to calibrate an equation of state for the reaction products. Wedge tests are used to determine the run to detonation distance of an explosive as a function of initiating shock pressure. This is done by optically measuring the reaction front on the wedge-shaped charge. Wedge tests will be discussed in detail in Chapter 4. Corner-turning tests measure the ability of an explosive to propagate at right angles to the axis of initiation [3]. This is important for explosives that are cast or machined into shapes that contain sharp corners. In the particle velocity gauge technique, a thin metallic foil (typically copper or aluminum) is placed inside an explosive charge, which is surrounded by a uniform magnetic field. Current is passed through the metallic foil and measured using an oscilloscope. When the shock wave impacts the metallic foil, the foil is accelerated to the same speed as the particles behind the shock wave. The voltage change due to electromagnetic induction in the foil moving through the uniform magnetic field is proportional to the

velocity of the foil and, consequently, the particle velocity behind the shock wave [2]. The particle velocity determined from the gauge measurements can be used to calibrate an equation of state for the unreacted explosive. Both the wedge and cylinder tests are large-scale and must be performed at outdoor ranges, while the corner-turning tests are usually laboratory-scale. Test charges implanted with electromagnetic particle velocity gauges can be small enough such that tests can be conducted in a large frag box or by using a gas gun, although some test charges are too large and require testing at an outdoor range.

Safety and cost concerns with typical large-scale experiments have motivated the design of small-scale characterization experiments. Three small-scale experiments that address corner turning are the mushroom test [4], Floret test [5], and the LLNL Tiny Plate test [6]. The mushroom test was developed at Los Alamos National Laboratory to investigate corner turning in insensitive high explosives (IHEs). Results from a mushroom test are a streak camera record of the detonation front as it emerges from the 1.0 inch diameter hemispherical sample. The shape of the streak record shows the detonation breakout angle, illustrating the explosive's ability to turn a 90° angle. Each mushroom test only uses about eight grams of test material. The Floret test is an even smaller derivative of the mushroom test, using a 4-mm thick, 12.7-mm diameter pellet of test material. Instead of accepting a shock wave from a donor explosive, the test pellet is impacted by an explosively-driven stainless steel flyer. This produces a shorter shock pulse than an explosive donor. The detonation spreads through the pellet and dents a copper plate attached to the pellet opposite the flyer impact. The dent in the copper is then used to determine the test material's corner

turning abilities. The LLNL Tiny Plate test does not consider breakout angle, but rather tracks a flyer plate accelerated by the test explosive with laser velocimetry. The test is similar in scale to the Floret and mushroom tests, with the test pellet measuring 5-mm thick and 6.35-mm in diameter.

None of these tests measure dynamic processes within the explosive. Both the mushroom test and Floret tests produce static measurements in the form of streak camera images and plate dents. While the LLNL tiny plate test does use laser velocimetry to track the velocity of the flyer, the detonation velocity is determined using the difference in time between the initiation of the test explosive and the breakout of the detonation on the flyer as sensed by the laser velocimetry. In order to achieve the goal of making dynamic measurements in a reacting explosive at the small scale, the technique of microwave interferometry is considered.

1.3 Microwave Interferometry

1.3.1 History

The first work using electromagnetic waves to track reactions in explosives was done by German scientists and engineers during WWII [7], although published record of this technique did not appear until 1953 by Koch [8]. Koch directed microwaves at a reacting charge and captured the reflections with an antenna. The waves were not directed at the reaction front and therefore recorded the dispersion of the detonation products. In 1955, Cook, Doran, and Morris [9] measured detonations of TNT, 50/50 Pentolite, 50/50 Amatol, and 80/20 Tritonal using a Michelson type interferometer. A horn antenna and metallic reflector were used to direct microwaves

and reflections from the interferometer underground to the explosive charge above. As noted by Cook, standoff measurements using antennas allowed for the propagation of multiple modes of the microwaves, distorting the results. Also in 1955, Boyd and Fagan [10] utilized a coaxial cable to transmit microwave data from the interferometer to a Composition B charge. These early studies used microwave wavelengths in the centimeter range and frequencies near 9 GHz. Favorable comparisons of microwave interferometry data to pin probe data in early study studies showed the validity of the technique.

Cawsey et al. [11] conducted a comprehensive study of detonation measurements with microwave interferometry. Experiments were conducted on explosives confined in small metal tubes such that a single mode of the microwaves was propagated. The evidence of unwanted reflections appeared in the fringe shapes collected by the oscilloscope, allowing the authors to tune the setup to obtain high resolution and consistency compared to previous studies. The microwave frequency used was 34.5 GHz and wavelengths were in the millimeter range; this provided better time resolution with appropriate waveguide dimensions than the Q-band microwaves used in previous studies. Detonation experiments were conducted on tetryl to demonstrate the technique. Cawsey et al. also showed microwave interferometry could observe the transient process in abrupt density change and growth to detonation. The growth to detonation observed by Cawsey et al. compared well to those observed experimentally by Berets, Green, and Kistiakowsky [12, 13] and a theoretical model developed by Eyring et al. [14].

Further development of the microwave interferometry technique in the 1960s and 1970s came from Johnson [15, 16], Saito [17, 18], and Alkidas et al. [19]. Johnson modified typical MI setups by physically attaching waveguides to the unconfined explosive charge, using the explosive itself as a dielectric rod. Johnson also observed the shock-to-detonation transition of Composition C-4 by placing a Plexiglas® card gap between sections of explosive. Results compared well with streak camera measurements. Another setup was presented by Saito, who measured microwave reflections from both sides of a gaseous detonation to extract information on the plasma physics. Alkidas et al. employed a quadrature mixer in the microwave interferometer setup. By measuring the phase angle between the reflected signal and the quadrature output signal to determine the reflected signal's frequency, the resolution of the measurement was greatly increased. Before this technique, the frequency of the reflected signal was determined using signal maxima, minima, and zero-crossing points. This limited the time resolution of the measurement to one quarter of the reflected signal's frequency, or 90° of the signal phase. The instruments used by Alkidas et al. were able to measure the phase angle relationship within 0.2°. The technique used by Alkidas et al. – known as quadrature analysis – was used in many subsequent studies, including Janesheski [20].

It is well known that microwaves are reflected by dielectric discontinuities. Initial studies on explosives using microwave interferometry made the assumption that the microwaves were strongly reflected by a highly-ionized plasma present in the reaction zone of the explosive. The degree of ionization is such that the plasma is highly conductive and acts as a "metallic sheet" that almost completely reflects the

incoming microwaves. In 1986, Anicin et al. [21] challenged this assumption while measuring solid propellant regression rates. Anicin et al. argued that the dielectric discontinuity at the solid-gas interface, not the highly-ionized reaction zone, was the mechanism responsible for reflecting the microwaves. To demonstrate this assertion experimentally, Anicin et al. sent microwaves through a solid propellant flame. No microwave reflections were captured even though the flame was a highly-ionized medium. Krall et al. [22, 23] responded to this new idea in 1993 by examining reacting and non-reacting shock waves in a piston impact experiment. Results from the non-reacting experiment showed the density gradient caused by the shock wave was sufficiently large to partially reflect the microwave signal. The portion of the signal not reflected by the shock wave traveled through the rest of the material and was completely reflected by the metal piston. This behavior was observed in the reacting material until it began to transition from deflagration to detonation (DDT). Once the reacting front appeared, the piston reflection vanished, indicating that all of the microwaves were either reflected or absorbed by the reaction. The signal amplitude reflected by the reaction started off much smaller than the piston signal amplitude, but grew to about the same level as the piston signal amplitude as the reaction reached steady state. This was explained as an increase in the density of hot spots as the material transitioned to detonation. The scattered hot spots do not provide sufficient ionization to be reflecting, but rather are dominated by a lossy mechanism due to the complex portion of the dielectric constant. Once the reaction fully develops, the dense ionization in the plasma results in almost total reflection of the microwaves. While there is still some disagreement on the exact mechanism of microwave

reflection, it is clear that reflection occurs at the shock wave or reacting front, and the method is valid for its intended purpose.

Researchers continue to use microwave interferometry to study reactive processes in energetic materials. Rae et al. [24] made improvements to the standoff MI technique by implementing a highly-directional antenna for a 34 GHz interferometer. The setup was used to observe detonation and run-to-detonation in PBX 9501. Results were within 0.03 km/s of those predicted by CHEETAH and a detailed description of the run-to detonation process as observed in the microwave signal was provided. Janesheski [20, 25] utilized a 35 GHz microwave interferometer and quadrature analysis to observe detonation failure in non-ideal explosives based on ammonium nitrate (AN). The failure rate of AN mixed with diesel fuel and mineral oil was characterized for varying levels of confinement.

1.3.2 Theory

Interferometry is a measurement technique based on interference. When radiation takes multiple paths from the source to the point of detection, the intensity oscillates about the sum of the intensities for each path. The result is light and dark bands collected at the source, known as interference fringes. The fringe position and/or visibility can be measured to deduce information about the path of the radiation. The applications of interferometry are numerous and range from measuring the speed of a small piston to measuring the diameter of a distant star [26]. Microwave interferometry utilizes radiation in the microwave range of the electromagnetic spectrum. In practice the wavelengths used tend to be in the

centimeter and millimeter range [26]. This method has been used extensively to track shock waves and detonations in explosives for many reasons, including that heterogeneous explosives often have desirable dielectric properties for microwave transmission [11], and the frequency and wavelength range matches the resolution requirements. While the technique was originally developed using radiation in and near the visible spectrum, there is no fundamental difference between an optical and microwave interferometer [27].

The basic operation of a guided wave microwave interferometer (where waves are transmitted in waveguides rather than through free space) tracking a shock wave is described as follows. The microwave signal is transmitted from the microwave source to the shock wave via a waveguide. When the signal encounters the shock, it is reflected back to the instrument due to a dielectric discontinuity. As discussed in the previous section, dielectric discontinuities are, in this case, the result of density gradients caused by the shock wave moving through a compressible material. If the material behind the shock wave is reacting, the dense, highly-ionizing plasma creates a reflecting "metallic sheet" that almost completely reflects the microwave signal [22]. The reflected signal then travels back to the instrument, where it is mixed with a reference signal to produce an interference signal. Because the shock wave is moving, the interference signal exhibits a Doppler shift proportional to the shock velocity [9]. Using the signal frequency and the microwave wavelength in the material where the reflection occurred, the velocity of the moving surface can then be determined by using the following relation [11]:

$$v = \frac{\lambda}{2} f \tag{1-1}$$

where λ is the wavelength of the material, f is frequency, and v is velocity. The process used to determine λ will be discussed in section 2.2.3. Finally, the position of the shock can be determined by integrating frequency with respect to time:

$$\mathrm{x} = \frac{\lambda}{2} \int_{t_1}^{t_2} f \, dt \tag{1-2}$$

Since microwaves in this setup are transmitted via waveguides, there is a limit to which signal modes can be transmitted based on the waveguide geometry. Transmission of a single mode is desirable to prevent distortions to the output signal [9] [11]. For waveguides modelled as circular pipes, the lowest frequency that can propagate through a waveguide of radius R is,

$$f_c = \frac{c}{3.413R\sqrt{K}} \tag{1-3}$$

where c is the speed of light and K is the relative permittivity of the space filling the waveguide. Above this cutoff frequency, the next fundamental mode of transmission occurs at the frequency f_c',

$$f_c' = \frac{c}{2.613R\sqrt{K}} \tag{1-4}$$

Combining (1-3) and (1-4) gives the limit for transmission of a single frequency mode [11]:

$$\frac{c}{3.413R\sqrt{K}} \leq f \leq \frac{c}{2.613R\sqrt{K}} \tag{1-5}$$

CHAPTER 2. METHODS

2.1 Experimental Setup

The MI used in this setup was custom built by Electrodynamic of Albuquerque, NM. Two microwave sources, one at 8 GHz – 20dB and the other at 27 GHz – 17 dB, are mixed together to produce an operating frequency of 35 GHz. The microwave signal is transmitted to the explosive charge via an expendable 0.25 inch polytetrafluoroethylene (PTFE) waveguide. PTFE, with a dielectric constant of 2.1 [28, 29], provides excellent microwave transmission and low monetary cost. A quadrature mixer is employed to produce a duplicate of the interference signal offset by 90° in phase. The quadrature phase relationship of the signals can be used to measure the phase angle of the interference signal if the quadrature data analysis method is used. The microwave circuit and microwave interferometer unit are shown in Figure 3 and 1

The explosive charge consists of the test explosive TATB, manufactured by BAE Systems (Lot #BAE12K296-009, ID #13-11-84-1112-110), and a booster, Ensign Bickford Primasheet® 1000. Loose TATB powder is pressed using a Carver model 3851-0 hydraulic press and custom die into 304 stainless steel pipes with 0.2565 inch ID and 0.028 inch wall thickness. The explosive charge is initiated by a Teledyne Risi, Inc. RP-501 Exploding Bridge Wire (EBW) detonator and Dyno-Nobel Primaline 4HS Detonating Cord (Case ID #0K0500079107). 3.5 feet of

detonating cord is initiated by the RP-501 in an external fragmentation containment pipe and travels into the main frag box to initiate the main explosive charge. The det cord provides a 152.4 μsec delay between the initiation of the RP-501 and the main explosive charge. This delay mitigates interference in the data collection system caused by the electromagnetic pulse from the Teledyne Risi, Inc. FS-62B EBW Firing Unit. Time-of-arrival measurements are made using Thorlabs, Inc. DET10A photo-detectors and M34L02 patch cables. The output from these signals will be used to calibrate wavelengths during data analysis. All data was collected at 2.5 GHz sampling frequency using a Tektronix DPO4034 Digital Phosphor Oscilloscope.

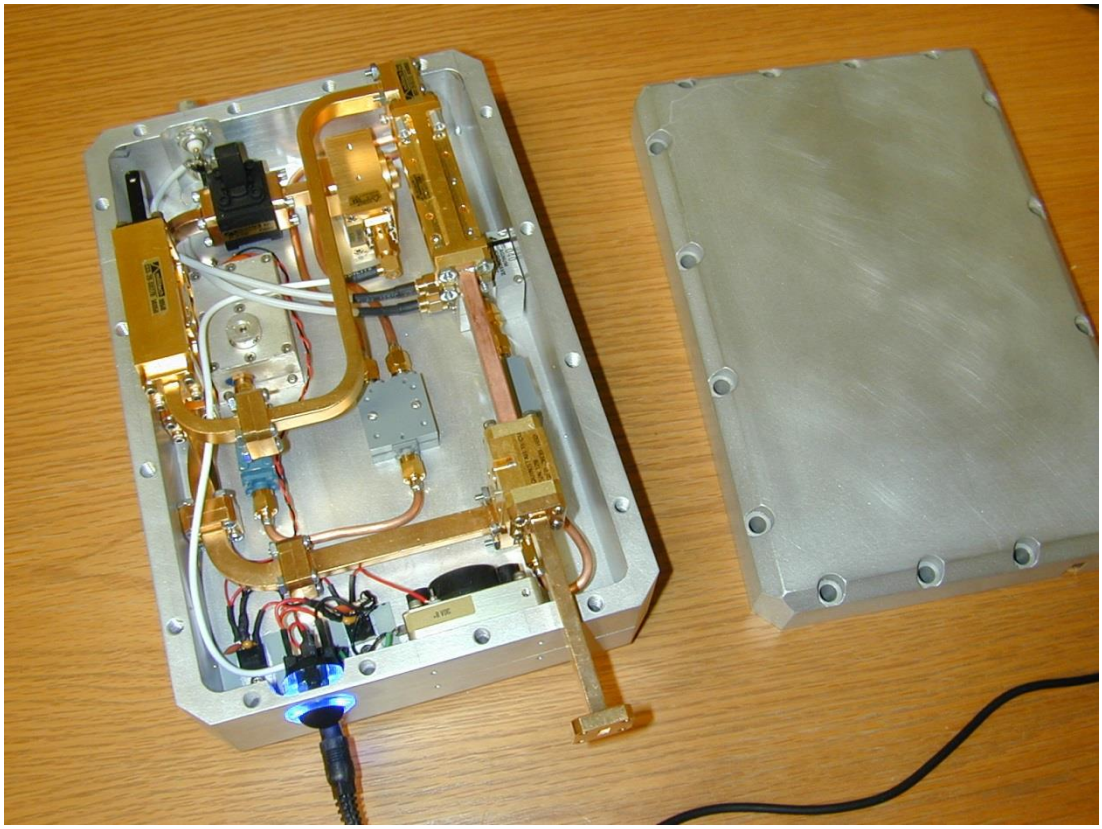

Figure 1: Microwave interferometer with top cover removed

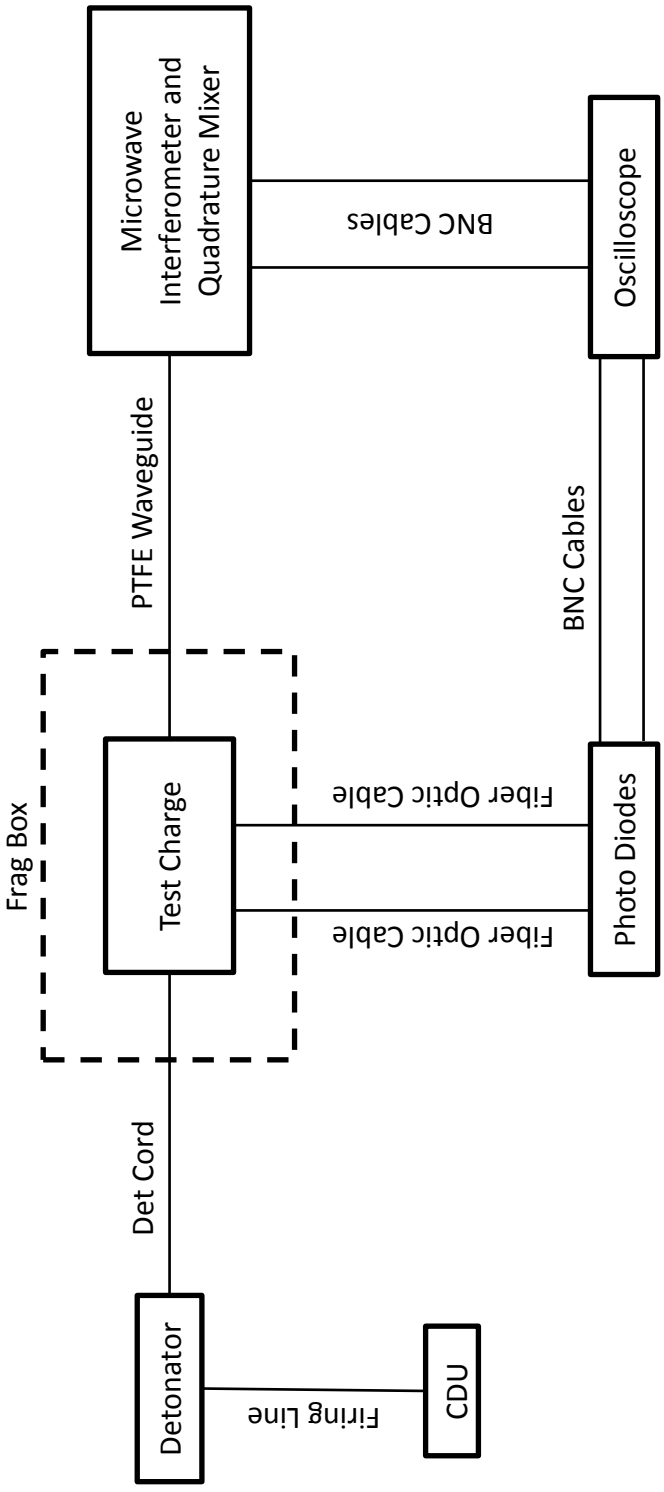

Figure 2: Block diagram schematic of experimental setup

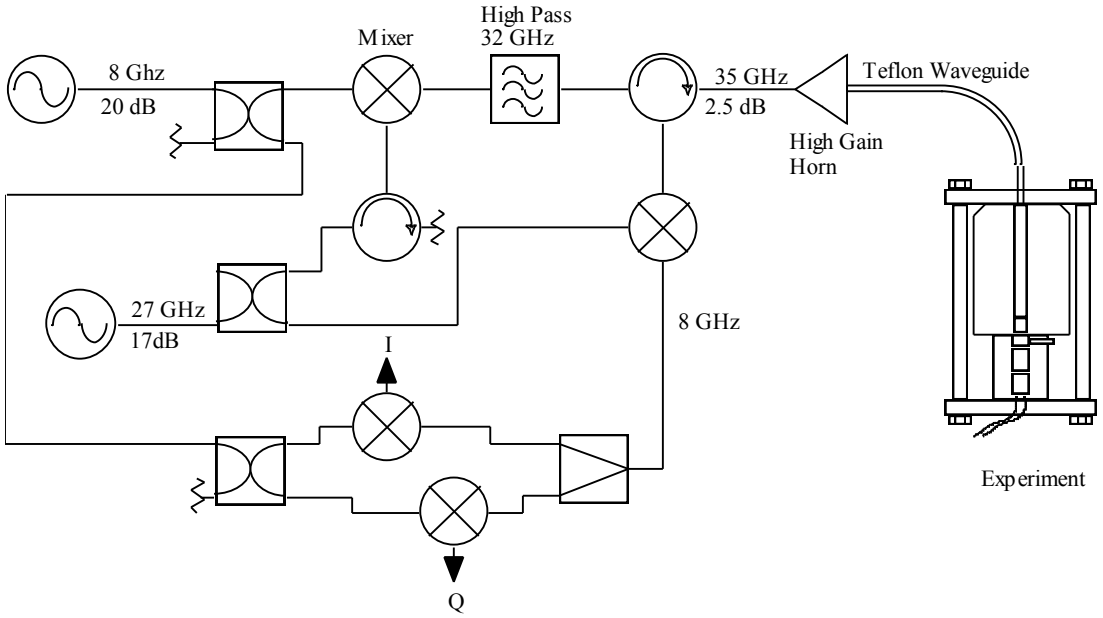

Figure 3: Microwave circuit for the microwave interferometer [30]

2.2 Data Analysis

2.2.1 Typical Result – Raw Data

A typical result collected using the oscilloscope is shown in Figure 4. The onset of the booster ignition is shown as the sinusoidal signal appears in the MI output channels. As the reaction moves through the charge, the amplitude of the MI output steadily increases up to about 7.0 mV. The reason for this increase is two-fold. First, the amplitude of the interference signal depends on the strength of the reflection that occurs at the dielectric discontinuity. In our case, the stronger and more planar the reaction front, the stronger the reflection [22]. As such, the amplitude of the signal increases as the reaction front of the booster develops. Second, both the booster and test material have dielectric losses associated with their complex permittivity. Because of this, the strength of the microwave signal is depleted slowly as it travels through more of each material. It follows that as the material is consumed the dielectric loses decrease and the signal strength increases. The reaction front strength

is responsible for the large amplitude increase in the booster portion of the test, while material consumption accounts for the steady growth in amplitude through the remainder of the test.

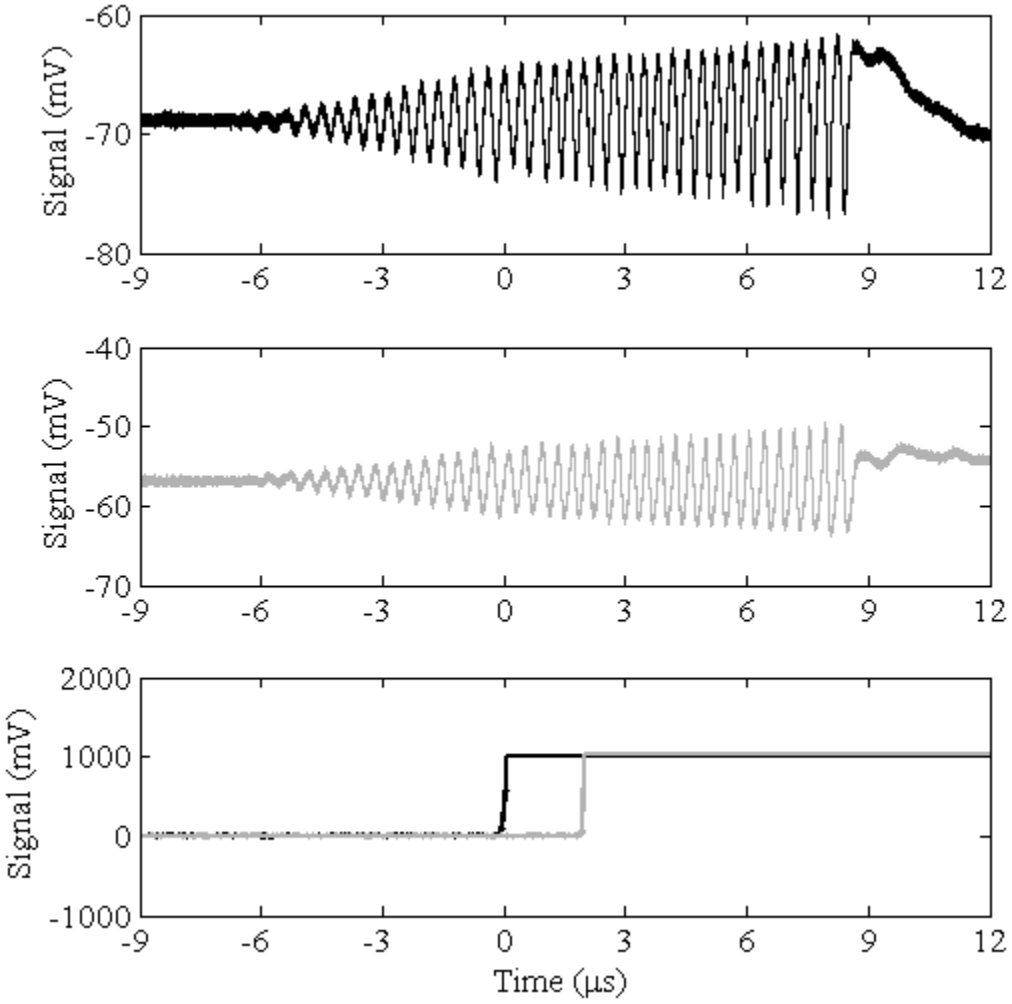

Figure 4: Raw signal from MI: original interference signal (top), quadrature mixer output signal (middle), and photo diode time-of-arrival traces (bottom)

The response of the fiber optic cables and photo diodes can also be seen in Figure 4. These measurements double as a trigger for the digital oscilloscope and time-of-arrival points that are used to determine the wavelength of the test explosive.

Note in this view the 90° phase shift of the MI output signals. This is the result of the quadrature mixer discussed earlier. Previous work [20] utilized the quadrature output to determine the position of the reaction front or shock wave using the phase angle between the signals. An alternative data analysis technique used in this investigation – wavelet transforms – is discussed in the following section.

2.2.2 Wavelet Analysis

Wavelet transforms are a type of numerical transform that extract the time-frequency components of signals. This type of transform was first proposed by Dennis Gabor in the 1940s [31], and was formalized by Grossmann and Morlet [32] to analyze signals used to study geophysical layers. The continuous wavelet transform of *f* at any scale *s* and position *u* is the projection of *f* on the corresponding wavelet atom, defined by equation (2-1):

$$Wf(u,s) = \int_{-\infty}^{\infty} f(t) \frac{1}{\sqrt{s}} \psi^* \left(\frac{t-u}{s} \right) dt \tag{2-1}$$

where ψ is the mother wavelet and "*" denotes the complex conjugate. There exist a number of different mother wavelets, each with its own tuning parameters. To determine the instantaneous frequency at each point in time, a normalized scalogram is calculated from the wavelet transform. The equation for the normalized scalogram is shown in equation (2-2).

$$N_W f(u,s) = \frac{|Wf(u,s)|^2}{s} \tag{2-2}$$

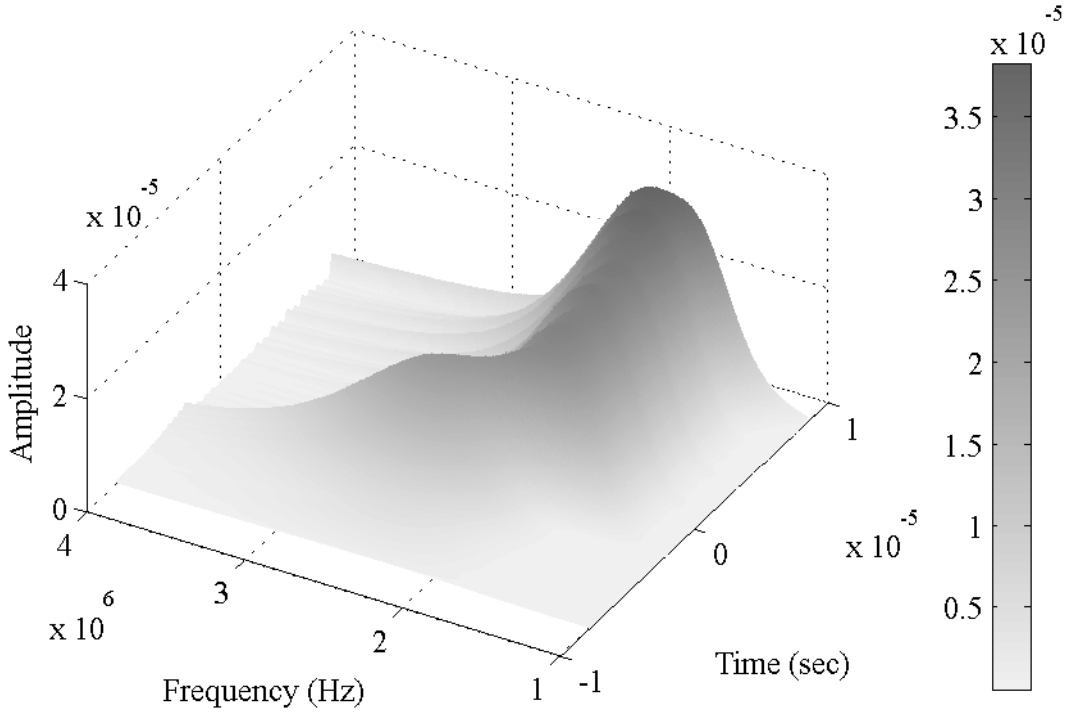

Figure 5: 3-D normalized scalogram

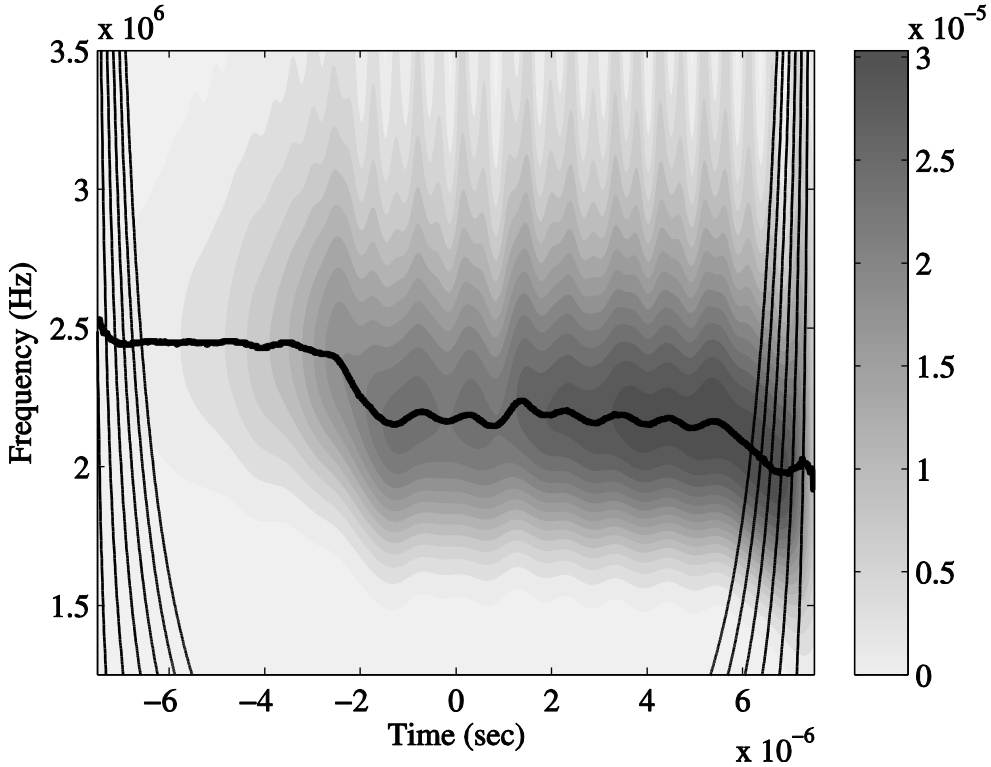

Figure 6: 2-D normalized scalogram with ridge result

The normalized scalogram is a 3-D array of time, frequency, and intensity of the signal [33]. The specific time-frequency relationship is extracted by finding the most intense frequency component of the signal at each point in time. The most intense frequency component of the signal with respect to time is known as the ridge of the signal [34]. An example of a 3-D scalogram is shown in Figure 5, and a 2-D scalogram with ridge result (the black line through the center) superimposed is shown in Figure 6.

Two corrections are necessary when using a wavelet transform. First, there is a "windowing" or "edge" effect associated with the determination of instantaneous frequencies. If two different dominant frequencies are located adjacent to each other in time, they both influence the determination of the dominate frequency at that time. The effect is also seen when the wavelet is integrated beyond the length of the signal. This smears the ridge across a wider time interval than where the frequency is actually present. The effect is negligible when the frequencies are similar, but becomes noticeable when there are sharp discontinuities in instantaneous frequency, making it harder to resolve these jumps. This is most problematic at both the beginning and end of the signal. To determine where the edge effect becomes significant, a calculation is done to determine the "radius of trust" of the ridgeline analysis [35]. The radius of trust equations for the Gabor wavelet are

$$\hat{f}(t_i + R) = k\frac{Gs\sqrt{2}}{4\pi R} \tag{2-3}$$

and

$$\hat{f}(t_f - R) = k\frac{Gs\sqrt{2}}{4\pi R} \tag{2-4}$$

where k is the multiple of the time spread [36]. In Figure 6, the parabolic curves on the left and right sides are the radius of trust for several k values. A value of k = 3 or 4 is typically recommended unless the signal has large amplitude variation or is highly damped [36].

The second correction is a frequency shift correction factor. If the wavelet does not satisfy the admissibility condition (that is, the function does not have zero mean with localized signal content about the origin [33]), there may be error in the frequency calculated using the wavelet transform. The equation for the frequency shift determined by [37] for the Gabor wavelet is

$$f = \left(1 + \frac{1 - \sqrt{2/Gs^2 + 1}}{2\,Fs}\right) f_o \tag{2-5}$$

where f is the true frequency and f_o is the pseudo frequency.

The wavelet transform analysis code used in this work was developed by Kittell and Mares et al. [38]. This program uses the Gabor mother wavelet, shown by equation (2-6) and Figure 7.

$$\psi(t) = \frac{1}{(\sigma^2\pi)^{1/4}} e^{-t^2/2\sigma^2} e^{i\eta t} \tag{2-6}$$

The Gabor mother wavelet was chosen because it is well documented in the literature [33] and requires the tuning of only a single parameter “Gs”. Using data taken from experiments similar to those presented in this paper, Kittell and Mares et al. [38] conclude that Gs = 4 is best suited for the application. By importing raw test data, the analysis is performed as follows:

1. The Gabor wavelet is calculated for the data
2. The continuous wavelet transform is calculated along with complex coefficients

3. The normalized scalogram is calculated and then filtered using a 3-D Savitzky-Golay filter [39] to remove artificial surface roughness
4. Ridge analysis is done to determine instantaneous time-frequency data
5. Radius of trust and frequency correction calculations are performed, and the final result is determined

The result of the wavelet transform code is given in terms of frequency. To convert this data to velocity and position, the wavelength of the test explosive must be determined. As discussed previously, velocity is directly proportional to wavelength, so great care must be used to determine this value.

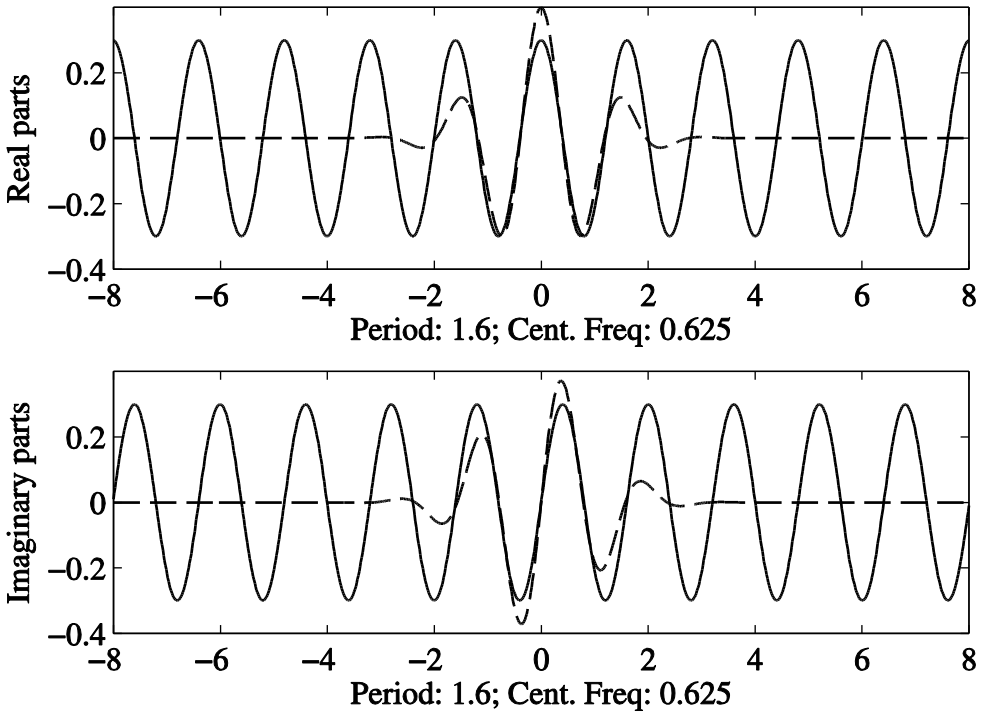

Figure 7: Gabor wavelet shape (dashed line) fit to a sine wave (solid line)

2.2.3 Wavelength Determination

As discussed in section 1.3.2, advancement in phase of 2π of the MI signal represents a displacement of the reflecting surface a distance of one characteristic microwave wavelength. Determination of this wavelength is critical to extract the velocity and position from the MI signal. In electromagnetic theory, the material's wavelength is a function of its relative permittivity by the relation [11]:

$$\lambda_g = \lambda_0\{\epsilon_r - (\lambda_0/\lambda_c)^2\}^{-1/2} \tag{2-7}$$

where λ_0 is the free space wavelength, λ_c is the cutoff wavelength of the empty confinement tube (λ_c = 3.413*R), ϵ_r is the relative permittivity of the material, and λ_g is the material wavelength. While ϵ_r is readily found for pure materials in the literature, heterogeneous mixtures require the use electromagnetic mixing equations to determine the contribution of each constituent to the relative permittivity of the mixture. Many mixing relations are available in the literature, and choice depends on material characteristics and application. The Landau-Lifshitz/Looyenga (LLL) equation [40, 41] will be used for this investigation. The LLL equation has been used in previous studies involving reacting porous media [22] and is valid for material where particle size is greater than 50 μm [42]. The relation for a material with two constituents is

$$\epsilon_r^{1/3}(mix) = \left(\epsilon_{r_A}^{1/3} - \epsilon_{r_B}^{1/3}\right)V_A + \epsilon_{r_B}^{1/3} \tag{2-8}$$

where ϵ_r(mix) is the relative permittivity of the mixture, subscripts A and B refer to each component (in this case, TATB and air), and V_A is the volume fraction of component A.

It is possible to determine the material wavelength experimentally using the MI. Since the displacement of the reflecting surface is proportional to the material wavelength, the wavelength can be calculated by collecting time-frequency data over a known distance. Integrating equation (1-1) with respect to time yields the relation to determine wavelength:

$$L_{1\to 2} = \frac{\lambda_g}{2}\int_{t_1}^{t_2} f(t) \tag{2-9}$$

where $L_{1\to 2}$ is the known distance, t_1 and t_2 are the time of arrival at the beginning and end of the known distance, and f(t) is the time-frequency of the signal found using the wavelet transform. Using this technique, the wavelength for TATB at varying density was determined and compared to theoretical predictions from the LLL equation. Results are shown in Figure 8.

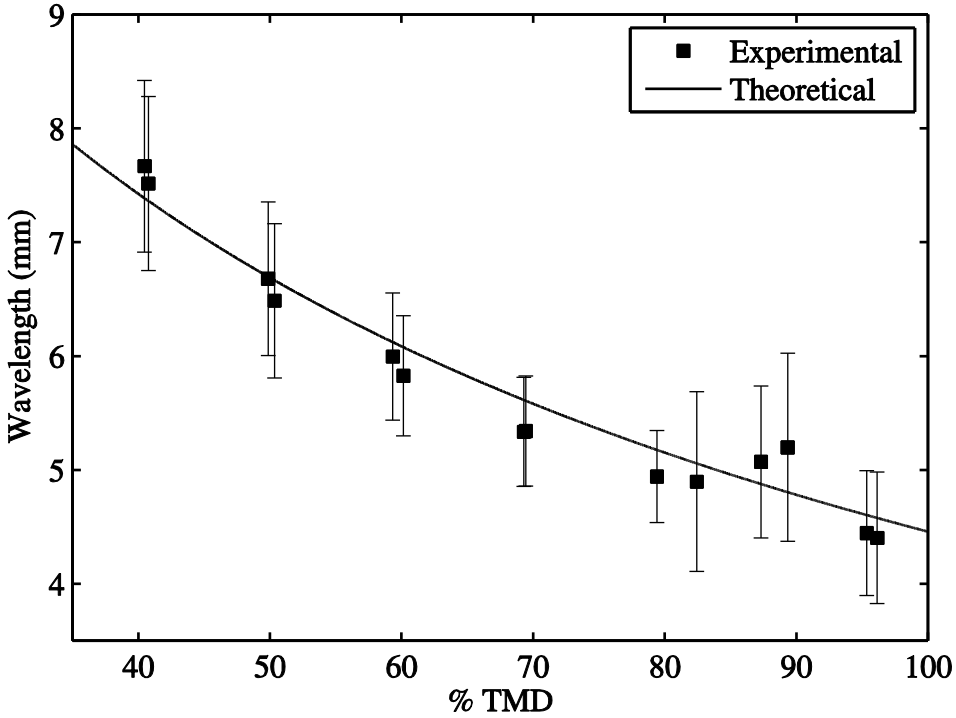

Figure 8: Comparison of theoretical and experimentally determined wavelengths

The experimentally determined wavelength agrees closely with the theoretical prediction within the error of the measurement. Since TATB is well-studied, the theoretical wavelength will be used to determine position and velocity in this investigation. The results discussed here demonstrate the capability of this experiment to determine wavelength in materials where dielectric properties are not well understood.

CHAPTER 3. RESULTS AND DISCUSSION: POROSITY STUDY

A series of charges packed with TATB of varying porosity were detonated to resolve the changes in detonation velocity. Increments of 10% TMD between each test grouping were desired, although some variation exists due to errors during charge preparation and pressing. A test matrix is shown in Table 1. Two tests were conducted at each density interval to confirm repeatability. Two additional tests were performed on 50% TMD TATB due to an anomaly that will be discussed later. An X-t plot of the results is shown in Figure 9, and velocity is shown as a function of time in Figure 10. Note that time and position = 0 (zero) corresponds to the transition point between the booster and the TATB test explosive.

Table 1: Porosity study test matrix

Test	Actual % TMD	Actual Density (g/cc)
40% TMD, Test 1	40.76	0.790
40% TMD, Test 2	40.47	0.784
50% TMD, Test 1	49.86	0.966
50% TMD, Test 2	50.35	0.975
50% TMD, Test 3	50.15	0.971
50% TMD, Test 4	50.39	0.976
60% TMD, Test 1	60.15	1.165
60% TMD, Test 2	59.34	1.149
70% TMD, Test 1	69.45	1.345
70% TMD, Test 2	69.29	1.342
80% TMD, Test 1	82.44	1.597
80% TMD, Test 2	79.41	1.538
90% TMD, Test 1	89.34	1.731
90% TMD, Test 2	87.31	1.691
96% TMD, Test 1	96.15	1.862
96% TMD, Test 2	95.36	1.847

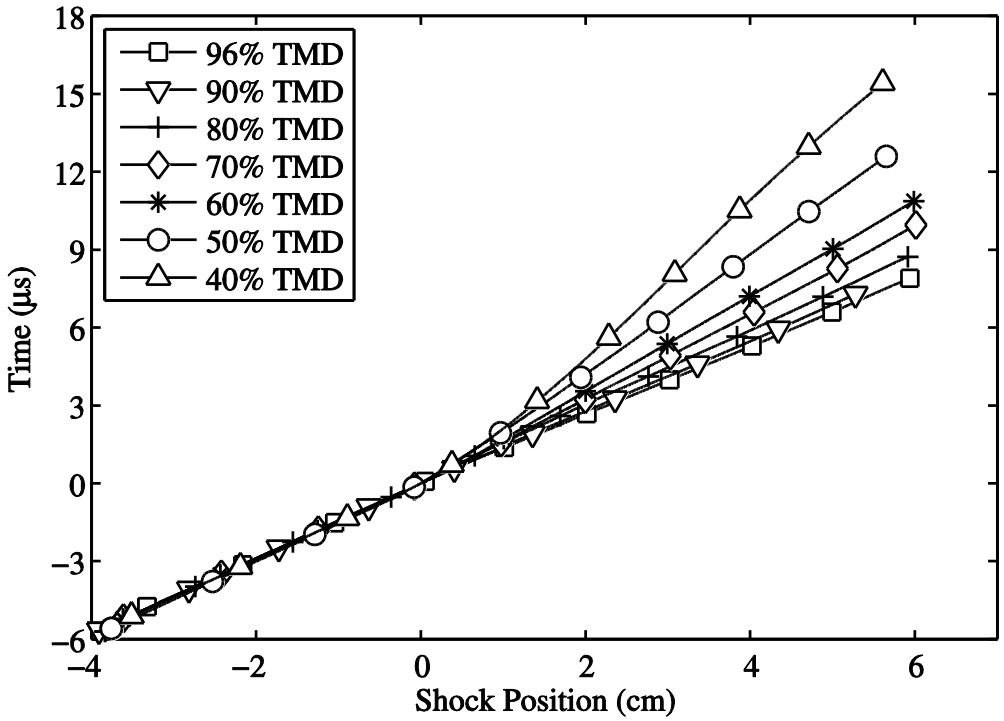

Figure 9: Porosity study, X-t plot

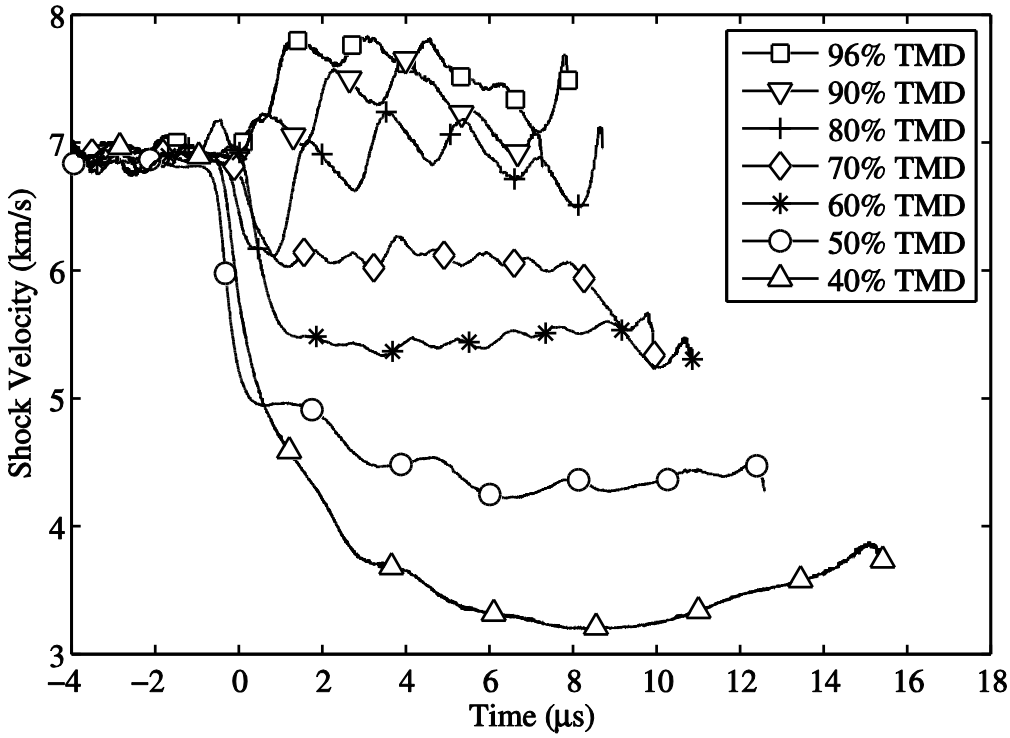

Figure 10: Porosity study, velocity vs. time

From Figure 10, there is a noticeable oscillation in the TATB velocity, especially for densities above 70%. This is a result of density gradients that exist due to the process of pressing the high density charges. The stainless steel confiner used in the experiment has a relatively thin wall thickness of 0.028 inches. The thin wall limits the hoop stress that can be applied to the confiner during pressing to about 27 ksi. This becomes problematic when pressing to higher densities. For tests conducted at 96%, 90%, and 80% TMD, the TATB was pressed in four increments of 0.5 inches ($L/D \approx 2$) and one increment of 0.25 inches ($L/D \approx 1$). The pressure applied to the 0.5 inch increments was not sufficiently large to compact the powder to uniform density. The density gradients in each pressing increment result in a velocity change through that portion of the charge. It can be seen that the velocity oscillations shown in Figure 10 correspond to each pressing increment. Previous versions of the wavelet transform analysis code were not able to resolve this phenomenon, and it was discovered only after the most recent and finely-tuned version of the analysis code was implemented. As a result of this discovery, tests conducted at 70% and 60% TMD were pressed using nine 0.25 inch increments. While density gradients still exist in these tests, the magnitude of the velocity oscillations is significantly decreased. The thin wall confiners were originally chosen because they were used in previous experiments [20, 25] without issue, albeit at lower pressing densities. Cost and availability also played a role in this confiner choice. The pressing effect could be easily mitigated in future tests by using more robust confiners to allow for higher pressing densities.

Looking at average detonation velocity, the results from the MI were compared to both theoretical predictions and empirical relations found in the

literature. The thermochemical equilibrium code CHEETAH [44] was used to calculate the C-J detonation velocity and inert material speed of sound for each test case. An empirical equation for infinite diameter detonation velocity as a function of TATB density from the Los Alamos Scientific Laboratory (LASL, now the Los Alamos National Laboratory) was used as a second comparison [43].

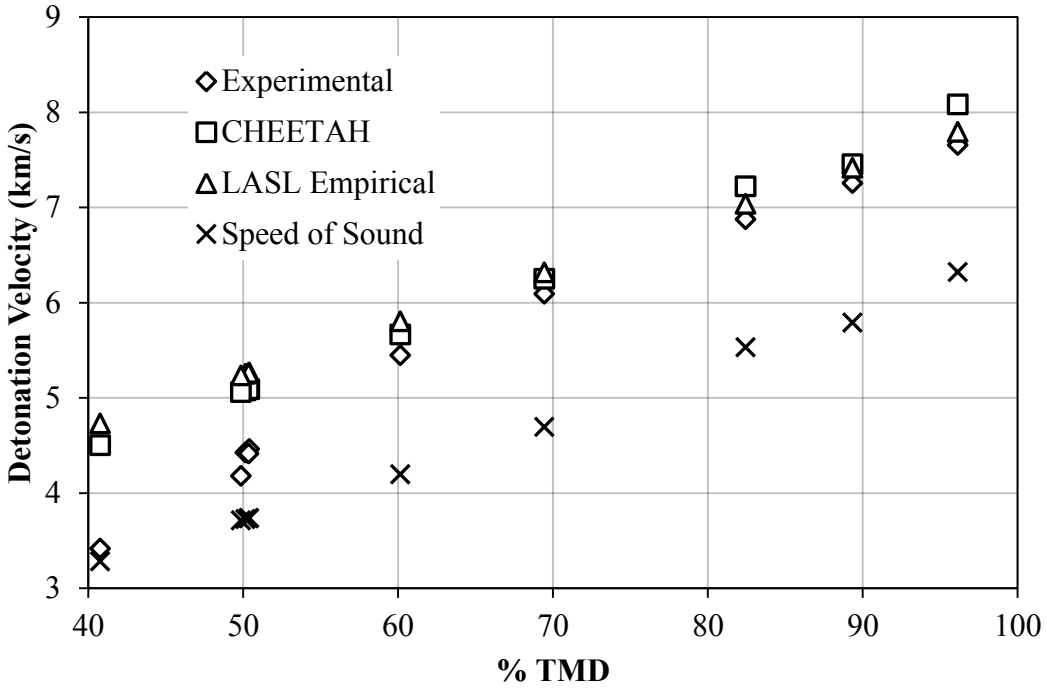

Figure 11: Comparison of experimental results with CHEETAH and Los Alamos empirical relations [43]

Figure 11 shows that the detonation velocity measured using the MI in TATB above 50% TMD compares well to those produced by the LASL relation and CHEETAH. Below 60% TMD, the measured velocity begins to deviate from the predictions. The average velocity for 40% TMD matches the inert material speed of sound predicted by CHEETAH. This suggests the material failed to detonate while an inert strong shock wave propagated though the TATB and confiner. No fragments or material

were recovered post-mortem, suggesting shock pressures were high enough to tear apart the confiner and scatter or vaporize the TATB. The absence of a reaction zone is also suggested by a marked decrease in MI signal amplitude once the shock wave reaches the TATB, shown in Figure 12. As discussed in section 1.3, the strong ionizing plasma found in a reaction zone is a stronger microwave reflector than an inert shock wave. The difference manifests in decreased amplitude of the reflected signal. This theory could be examined by using ionization pins to determine whether a reacting front accompanied the shock wave detected by the MI.

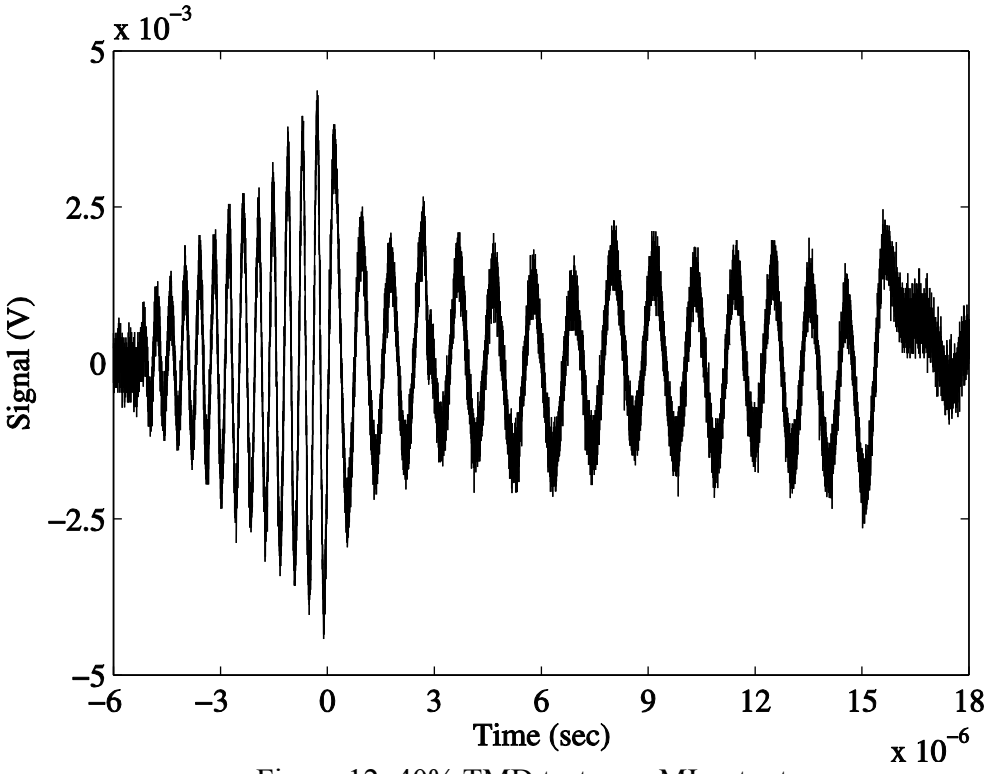

Figure 12: 40% TMD test, raw MI output

Figure 11 also shows that the measured average velocity in 50% TMD TATB lies between the predicted detonation velocity and inert material speed of sound. For the 50% TMD case in Figure 10 there are several points where the velocity appears to decrease in "steps." These variations do not correspond with pressing intervals like

those at higher densities. Additional tests conducted at 50% TMD are shown in Figure 13 and have similar steps in velocity. The number of steps, their position in time, and the magnitude of the velocity change varies from test to test with no discernable pattern. Comparing Figure 14 to Figure 13, we see that the steps in velocity data correspond to a decrease in the MI output signal amplitude. As with the 40% TMD case, this indicates a decrease in microwave reflection as a result of a dying reaction front. However, average velocities from the 50% TMD experiments do not match the material inert speed of sound. The discrepancy suggests that the reaction in the 50% TMD case has not yet died, but is losing energy as it propagates down the charge. In this process, energy losses to the sides of the confiner in the form of heat begin to overcome the energy produced by the reaction. The reaction begins to die as the energy lost becomes greater than the energy required to sustain the reaction. This process is not always instantaneous. The reaction can build and decline repeatedly as energy is lost and produced, resulting in a process known as “chugging.” Given enough test material length, the process should reach steady state, although the necessary length is not easily predicted. Additionally, it is not guaranteed that the material will detonate or fail each time. Under a set of fixed conditions, the end result of the test (detonation or failure) could be governed by a statistical distribution. There exists a setup where there is a 50% chance of “go” or “no-go.” Given a sufficiently long charge and an adequate number of tests, the statistical probability of “go” or “no go” for this setup at 50% TMD could be determined.

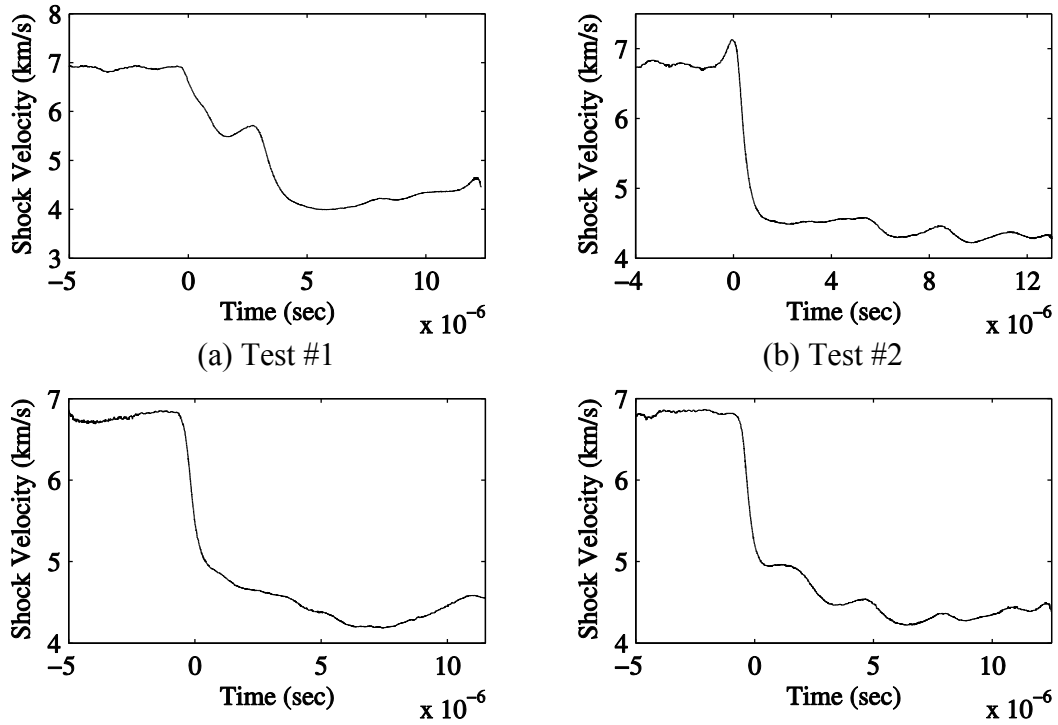

(a) Test #1 (b) Test #2

(c) Test #3 (d) Test #4

Figure 13: Velocity vs. time of additional 50% TMD tests

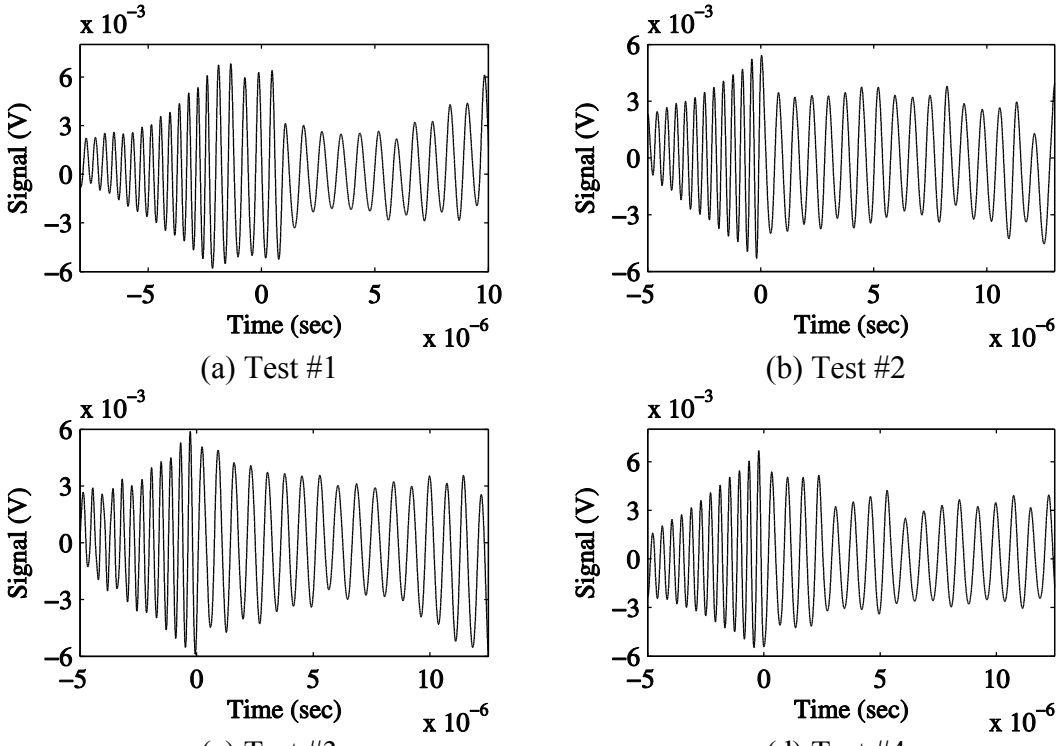

(a) Test #1 (b) Test #2

(c) Test #3 (d) Test #4

Figure 14: Raw signal of 50% TMD tests

CHAPTER 4. RESULTS AND DISCUSSION: SHOCK INITIATION STUDY

The shock initiation of TATB in the experimental configuration was investigated by placing a PMMA attenuator between the booster and test explosive to modify the pressure of the shock wave that initiates the TATB. PMMA was chosen because its sound speed is adequately small to attenuate the shock pressure down to desirable levels. Additionally, PMMA is a microwave transmitting material, which allows the shock wave behind the PMMA to be resolved. In contrast, metallic attenuators such as aluminum or brass would reflect microwaves at their surface such that only the shock in front of the attenuator could be resolved. For these investigations, the oscilloscope was triggered using a fiber optic cable placed at the detonator/det cord connection. This insured data collection even if the shock was attenuated to the point that the TATB failed to detonate. The test matrix is shown in Table 2.

Table 2: Shock initiation study test matrix

Test	Actual % TMD	Actual Density (g/cc)	Attenuator Length (mm)	Failure?
80% TMD Test 1	79.48	1.5396	5	NO
80% TMD Test 2	78.60	1.5225	5	NO
80% TMD Test 3	79.10	1.5321	7	YES
80% TMD Test 4	79.47	1.5393	7	YES
96% TMD Test 1	98.80	1.9137	1	NO
96% TMD Test 2	97.20	1.8828	1	NO
96% TMD Test 3	96.21	1.8635	3	YES
96% TMD Test 4	97.47	1.8880	3	YES

Two shots were conducted at one “go” condition and one “no-go” condition for each density to bracket the case, resulting in eight shots total. No-go’s were clearly indicated by a complete lack of microwave signal after the attenuator and recovery of the unreacted material in the frag box.

The raw output signal and shock velocity for all “go” tests are shown in Figure 15. The gray box on each plot represents the time during which the shock wave is travelling through the PMMA. Microwave reflection is weak in the PMMA since the shock wave does not produce sufficiently large pressure gradients to reflect the signal there. Hence, the dashed line in the velocity plots does not represent a velocity, but a linear fit between the point where the shock wave enters and exits the PMMA shown for visualization and coherence. For all tests, the microwave signal in the TATB has an amplitude of about 3-5 mV as the shock exits the PMMA, and then builds to an amplitude of about 12-15 mV. This is consistent with the mechanism discussed by Krall et al. [22] and in Chapter 2; the amplitude of the reflected microwave signal increases as the reaction forms behind the shock wave in the TATB. The amplitude of the signal also increases as more TATB is consumed, since TATB does absorb some of the microwave signal. A more in-depth explanation of the shock-to-detonation transition (SDT) process downstream of an attenuator observed using a microwave interferometer is given by Rae et al. [24] and shown in Figure 16. In their experiment, the MI signal was reflected by the front of the aluminum attenuator until the shock wave emerged. At this point, a majority of the microwaves were still reflected off the aluminum surface, the reflection from the shock wave being insignificant by comparison. Once the onset of thermal explosion appeared, more

microwaves were reflected off the reacting shockwave. Eventually the reaction reached steady state and the reacting plasma fully reflected the microwaves. The major difference between the current experiment and Rae et al. is that PMMA does not reflect microwaves, and therefore the smaller microwave reflections from the inert shock wave can be detected.

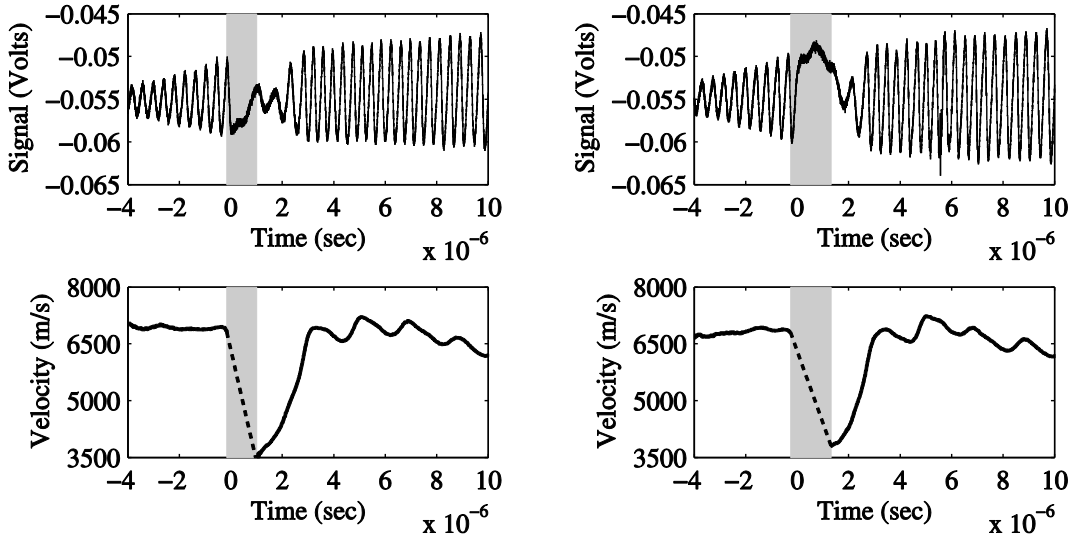

(a) 80% TMD, Test 1

(b) 80% TMD, Test 2

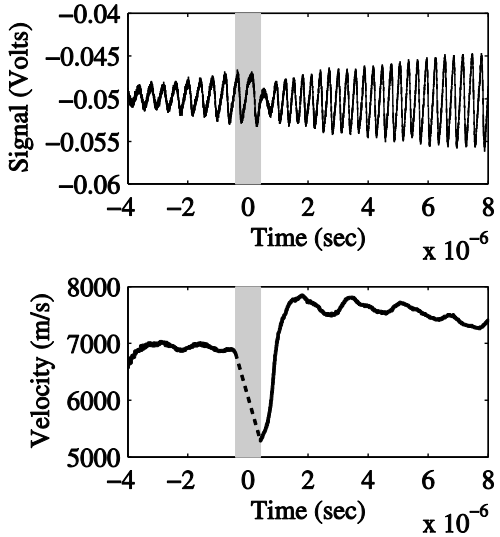

(c) 96% TMD, Test 1

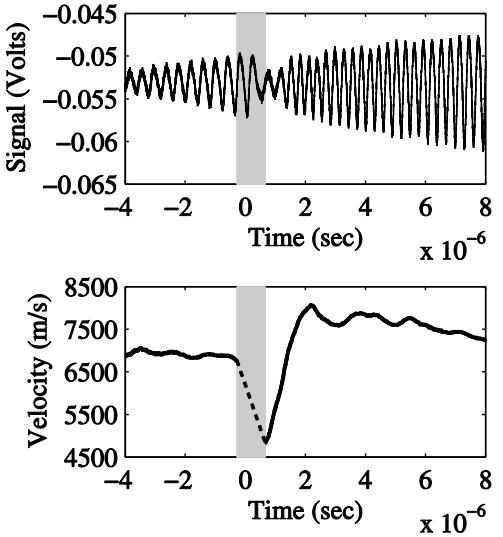

(d) 96% TMD, Test 2

Figure 15: Raw output signal and velocity vs. time for all "go" tests

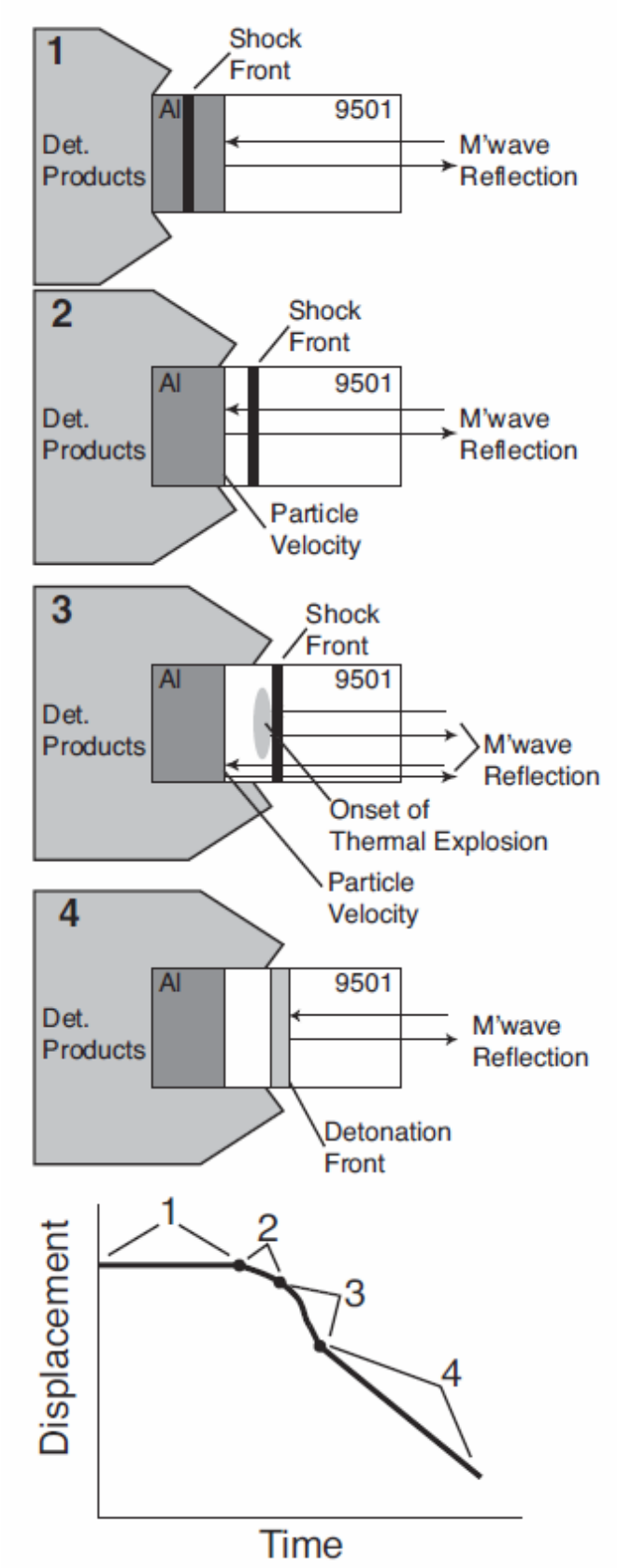

Figure 16: Shock-to-detonation transition from [24]

The position and velocity of all "go" tests are shown in Figure 17 and Figure 18. In general, test repeatability is good for each case. Some variation in the position/time of SDT onset does exist in a given test case. This is due to inherent uncertainty in choosing the time from the signal and velocity plots. It is not always clear when the reaction begins, and the fiber optic response at this point also has some variability. Use of shock and ionization pin sensors could be used in future experiments to better resolve this transition point. An example of a "no-go" test is shown in Figure 19. The remaining "no go" cases are not shown since the only data collected is that of the detonating booster. While it is well established that for most explosives (including TATB) there is a shock initiation pressure where the explosive will detonate 50% of the time [43], all tests in this work were repeatable. The 50% shock initiation condition could be found given additional time and resources, but that is not the objective of this study.

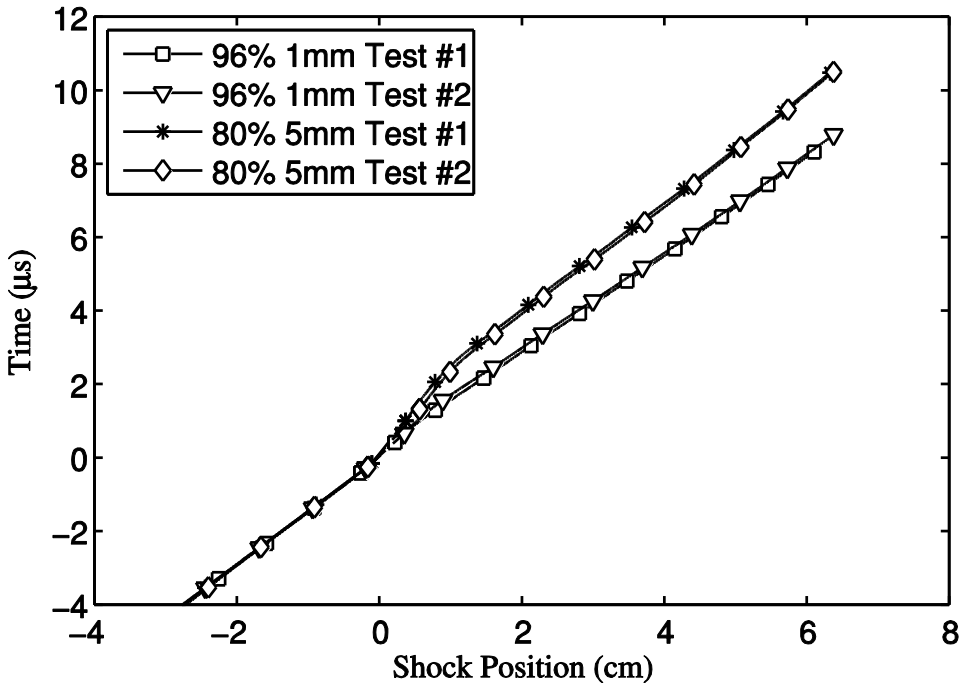

Figure 17: X-t plot of all "go" tests

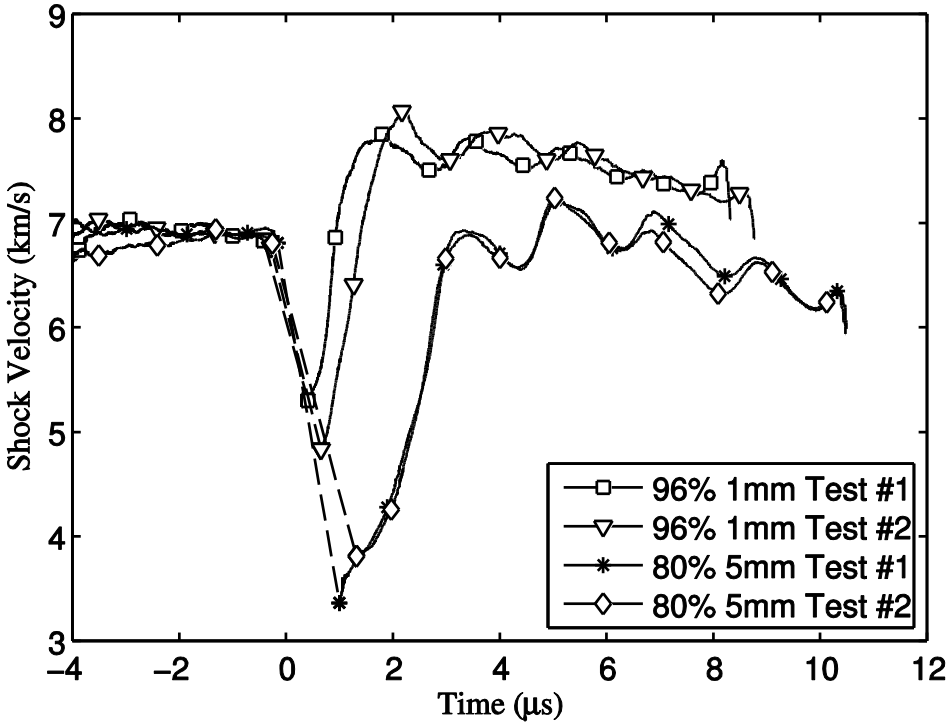

Figure 18: Velocity vs. time of all "go" tests

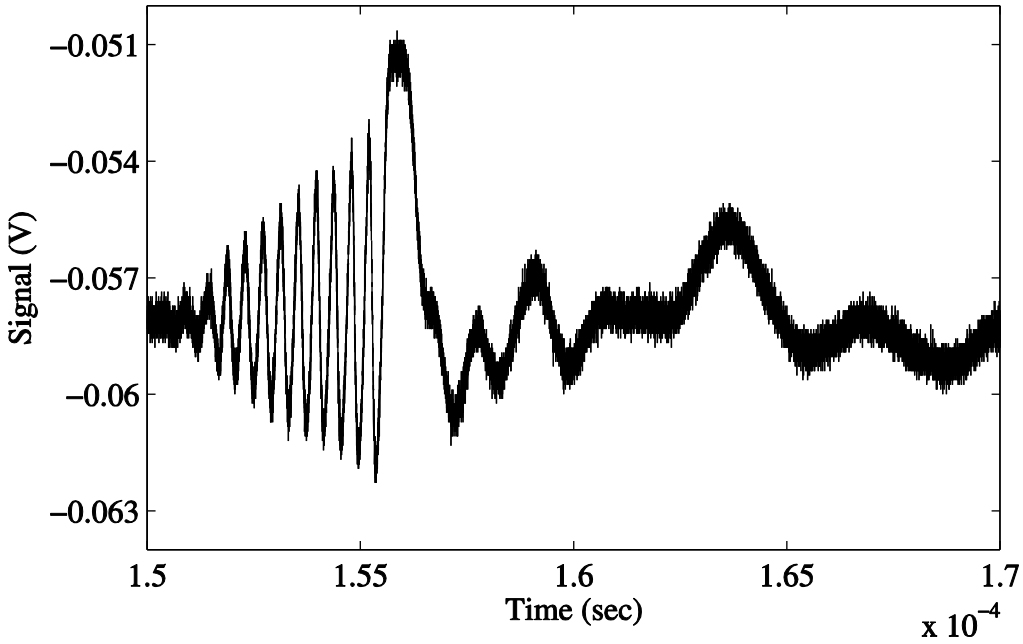

Figure 19: Raw output signal of "no-go" test

A secondary objective of this study was to determine whether this experiment could be used to obtain shock initiation pressures and run-to-detonation lengths of the test explosive. This data is typically obtained from wedge tests. The wedge test was developed by Majowicz and Jacobs [45], and Campbell et al. [46], and involves imaging the shock to detonation transition in a high explosive sample that is shaped like a wedge. A schematic of the typical wedge test is shown in Figure 20.

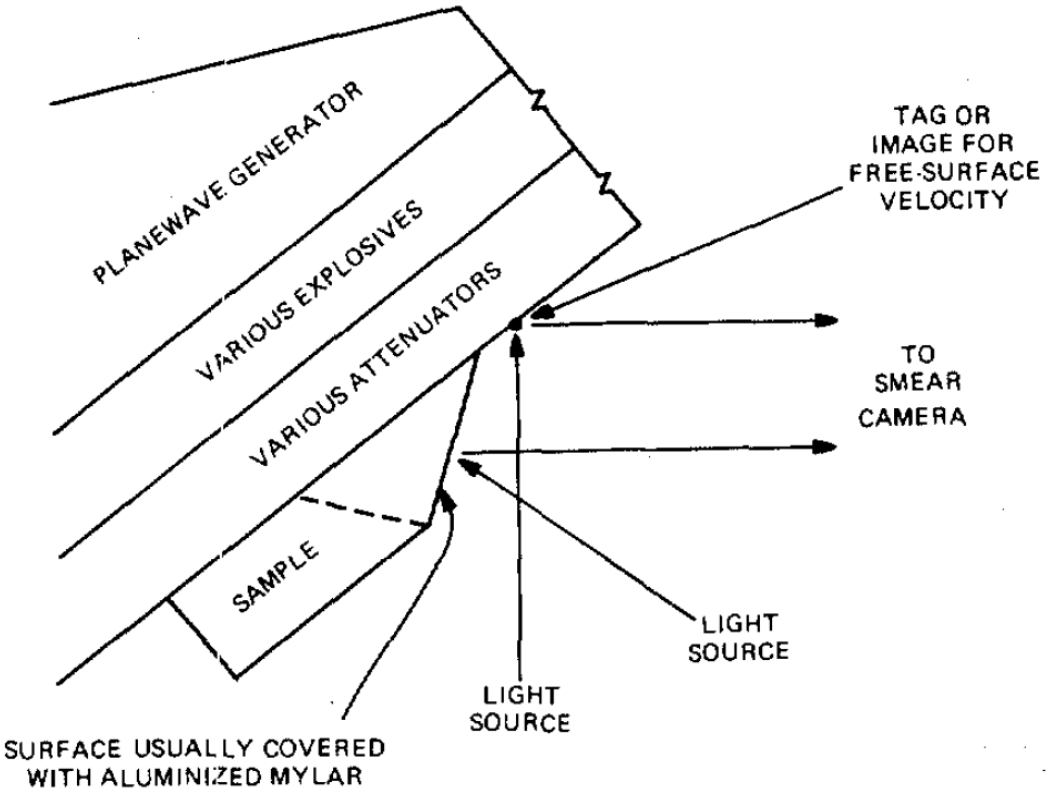

Figure 20: Typical wedge test setup, from [43]

The slanted side of the wedge is imaged using a streak camera, and the run-to-detonation distance is found using the images. The initiating shock pressure is set using a donor explosive and attenuator. Data from wedge tests is typically presented as shock initiation pressure versus run-to-detonation distance plotted on logarithmic

axes. This type of figure is called a “Pop”-plot, after former Los Alamos National Laboratory engineer Alfonse Popalato [47, 48]. The relation between shock initiation pressure and run-to-detonation distance is almost always linear on logarithmic axes, and it is customary to produce a logarithmic least-squares fit to the data.

For the present experiment, run-to-detonation distance was defined as the distance the shock wave traveled from the end of the attenuator to the position where it achieved its average detonation velocity. CTH was used to determine the initiating shock pressure after the attenuator. Results were compared to wedge test data from the Los Alamos Scientific Laboratory Explosive Property Data handbook [43] using the Pop-plot shown in Figure 21. Results show that both shock initiation pressures and run-to-detonation distances from the current experiment match the LASL data very closely, although the slope of the fit line for the current experiment is slightly larger. There are some aspects of the current test that must be considered when comparing to the wedge test. With regard to the wavelet transform analysis, there exists a “windowing” effect where frequency data adjacent to the time being analyzed can influence the result at that specific point in time. This is a result of the balancing act between time and frequency resolution discussed in section 2.2.2. Such an effect is exaggerated when there is an abrupt change in frequency (velocity), such as at the interface between the attenuator and test explosive. This effect could distort the run to detonation distance determined using this experiment. Outside of the data analysis, there are considerable differences in the scale and setup of these two tests. An example is that the experiment presented here was conducted with confinement, while a wedge test is not. It seems obvious that this would have an effect on the data,

although it is difficult to draw any definitive conclusions due to the limited sample size. More tests with additional materials would help to characterize the discrepancies.

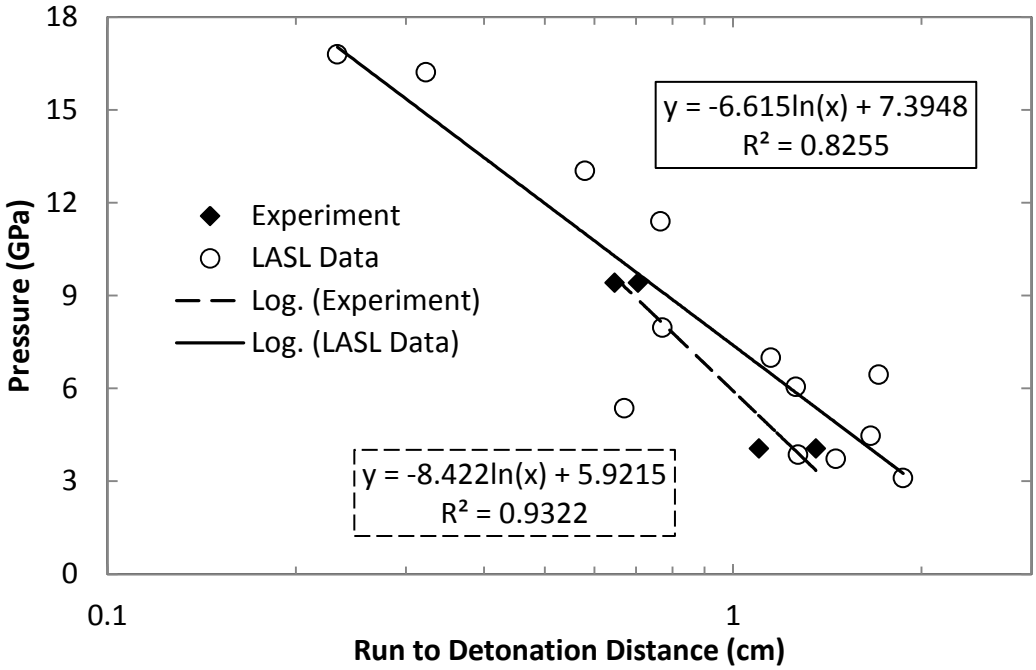

Figure 21: Pop-plot of experimental data and data from [43]

It should be noted that the level of agreement between the two results is exceptional given the significant differences in the experimental setups. The experiment presented here has a distinct advantage in its substantially smaller scale and requires fractions of the net explosive weight (NEW) associated with a wedge test. This greatly increases safety and reduces the cost and oversight necessary to perform the test. As such, this test has potential to serve as a first-order calculation of SDT characteristics before the material is scaled up to a full-sized wedge test. This is particularly advantageous if the material is sensitive and there are safety concerns with scale-up. The viability of this experiment as a wedge test alternative would be further reinforced by additional tests with other established energetic materials such as RDX, HMX, and PETN.

CHAPTER 5. CONCLUSIONS

Microwave interferometry was applied to a small-scale experiment used to determine detonation velocity and run to detonation distance. Experiments were performed using pressed TATB at a wide range of densities. Results from these tests were compared to values obtained from the literature and the thermochemical equilibrium code CHEETAH.

It was shown that MI and wavelet transform results can be used to experimentally determine the microwave wavelength of TATB. The experimentally-determined wavelengths matched the wavelengths predicted by the Landau-Lifshitz/Looyenga electromagnetic mixing equation within the error of the experiment. Although wavelengths used in this work to calculate position and velocity were found using the Landau-Lifshitz/Looyenga equation, the accuracy of the experimental technique shows that the experiment can be used to determine microwave wavelength if the material's electromagnetic characteristics are unknown or not easily predicted.

The detonation velocity of porous TATB found using the microwave interferometer matched the velocity predicted by CHEETAH and an empirical relation from the LASL. As porosity increased, the detonation became unstable and propagated at a speed lower than the predicted detonation velocity. Unsteady behavior manifested itself as sudden jumps in the amplitude of the MI signal and

detonation velocity. At sufficiently low density the TATB failed to detonate but sustained a shock wave that propagated at the material's speed of sound. The experiment was then modified to allow measurement of the run to detonation distance of TATB. This was achieved by placing a PMMA insert between the booster and TATB to attenuate the initiating shock pressure. A Pop plot of the data revealed that results from this experiment closely match data from LASL obtained using wedge tests.

Tests performed in this work use only grams of booster and test material. This is significantly less than traditional characterization tests – such as the wedge test – which typically require kilograms of material and must be performed at an outdoor test range. In explosives engineering, less material is synonymous with lower costs and increased safety. There are also hazards associated with outdoor testing, such as weather and hazard area control. The MI test addresses all of these issues. While full-scale testing is necessary to completely characterize a new material, the MI test setup has potential to serve as an alternative for early screening before the material production is scaled up.

The methods described in this work have only been demonstrated using TATB. Future work will begin with testing using other previously characterized materials to demonstrate the accuracy of the experiment beyond TATB. After the method is established, the experiment can be used to determine detonation velocities and run distance to detonation for new and improvised explosive materials. The long term goal for the project is to calibrate explosive models for these new and improvised explosives using data from the microwave interferometer.

LIST OF REFERENCES

LIST OF REFERENCES

[1] P. W. Cooper and S. R. Kurowski, Introduction ot the Technology of Explosives, Hoboken, NJ: Wiley-VCH, 1996.

[2] M. Suceska, Test Methods for Explosives, New York, NY: Springer-Verlag, 1995.

[3] M. Cox and A. W. Campbell, "Corner-Turning in TATB," in *Seventh Symposium (International) on Detonation*, Annapolis, Maryland, 1981.

[4] L. G. Hill, W. L. Seitz, C. A. Forest and H. H. Harry, "High Explosive Corner Turning Performance and the LANL Mushroom Test," in *Shock Compression of Condensed Matter*, Amherst, MA, 1997.

[5] K.-Y. Lee, J. E. Kennedy, L. G. Hill, T. Spontarelli and J. R. Stine, "Synthesis, Detonation Spreading, and Reaction Rate Modeling in Fine TATB," in *Eleventh International Detonation Symposium*, Snowmass, CO, 1998.

[6] J. L. Cutting, H. H. Chau, R. L. Hodgin, D. M. Hoffman, F. Garcia, R. S. Lee, E. McGuire, A. R. Mitchell, P. F. Pagoria, R. D. Schmidt, R. L. Simpson, P. C. Souers and R. W. Swansiger, "A Small-Scale Screening Test for HE Performance: Application to the New Explosive LLM-105," in *Eleventh International Detonation Symposium*, Snowmass, CO, 1998.

[7] B. C. Glancy and A. D. Krall, "Microwave Interferometric Measurements of Particle and Wave Velocities in Porous Media," Naval Surface Warfare Center, Silver Spring, 1990.

[8] B. Koch, "Reflexion de micro-ondes par des phenomenes de detonation," *French Academy of Sciences, Paris,* vol. 236, pp. 661-663, 1953.

[9] M. A. Cook, R. L. Doran and G. J. Morris, "Measurement of Detonation Velocity of Doppler Effect at Three-Centimeter Wavelength," *Journal of Applied Physics,* vol. 26, no. 4, pp. 426-428, 1955.

[10] T. J. Boyd Jr and P. Fagan, "A Microwave Technique for Measuring Detonation Velocities," in *2nd International Detonation Symposium*, Washington, 1955.

[11] G. F. Cawsey, J. L. Farbrands and S. Thomas, "Observations of Detonation in Solid Explosives by Microwave Interferometry," in *Proceedings of the Royal Society of London. Series A, Mathematical and Physical Sciences*, London, 1958.

[12] D. J. Berets, E. F. Green and G. B. Kistiakowsky, "Gaseous Detonations. II. Initiation by Shock Waves," *Journal of the American Chemical Society,* vol. 72, no. 3, pp. 1086-1091, 1950.

[13] D. J. Berets, E. F. Greene and G. B. Kistiakowsky, "Gaseous Detonations. I. Stationary Waves in Hydrogen-Oxygen Mixtures," *Journal of the American Chemical Society,* vol. 72, no. 3, pp. 1080-1086, 1950.

[14] H. Eyring, R. E. Powell, G. H. Duffey and R. B. Parlin, "The Stability of Detonation," *Chemical Reviews,* vol. 45, no. 1, pp. 69-181, 1949.

[15] E. G. Johnson, "A Microwave Technique of Deteromining Growth to Detonation," *AIAA Journal,* vol. 3, no. 11, pp. 2109-2111, 1965.

[16] E. G. Johnson, "A Microwave Technique for Studying Detonation Phenomena," in *4th International Detonation Symposium*, White Oak, 1965.

[17] K. Saito, "Measurements of the High Electron Density Zone in C2H2-O2 Detonation Waves by Microwave Reflection," *Combustion and Flame,* vol. 21, pp. 241-251, 1973.

[18] K. Saito and H. Yamamura, "Microwave Reflection from Detonation Waves in Equimolar C2H2-O2 at Low Pressures," *Combustion and Flame,* vol. 20, pp. 59-69, 1973.

[19] A. C. Alkidas, A. T. Clary, G. Giles and S. V. Shelton, "Measurement of Steady State and Transient Solid Propellant Burning Rates with Microwaves," Georgia Institute of Technology, Atlanta, 1973.

[20] R. S. Janesheski, "Detonation Failure Characterization of Non-Ideal Explosives," Purdue University, West Lafayette, 2011.

[21] B. A. Anicin, B. Jojic, D. Blagojevic, M. Adzic and V. Milosavljevic, "Flame Plasma and the Microwave Determination of Solid Propellant Regression Rates," *Combustion and Flame,* vol. 64, pp. 309-319, 1986.

[22] A. D. Krall, B. C. Glancy and H. W. Sandusky, "Microwave Interferometry of Shock Waves. II. Reacting Porous Media," *Journal of Applied Physics,* vol. 74, no. 10, pp. 6328-6334, 1993.

[23] A. D. Krall, B. C. Glancy and H. W. Sandusky, "Microwave Interferometry of Shock Waves. I. Unreacting Porous Media," *Journal of Applied Physics,* vol. 74, no. 10, pp. 6322-6327, 1993.

[24] P. J. Rae, B. B. Glover, J. A. Gunderson and W. L. Perry, "Free-Field Microwave Interferometry for Detonation Front Tracking and Run-to-Detonation Measurements," in *Shock Compression of Condensed Matter*, Chicago, 2011.

[25] R. S. Janesheski, L. J. Groven and S. F. Son, "Detonation Failure Characterization of Non-Ideal Explosives," in *Shock Compression of Condensed Matter*, Chicago, 2011.

[26] W. H. Steel, Interferometry, 2nd ed., New York, NY: Cambridge University Press, 1983.

[27] K. D. Froome, "Determinatin of the Velocity of Short Electromagnetic Waves by Interferometry," *Proceedings of the Royal Society of London. Series A, Mathematical and Physical,* vol. 213, no. 1112, pp. 123-141, 1952.

[28] Plas-Tech Coatings, "DuPont Teflon Industrial Coatings," Plas-Tech Coatings, West Chester, PA, 2002.

[29] M. E. Daily, "Electromagnetic Studies of Explosives at ISM (Industrial, Scientific, and Medical) Frequencies," Purdue University, West Lafayette, IN, 2013.

[30] N. J. Burnside, S. F. Son, B. W. Asay and P. M. Dickson, "Deflagration to Detonation Experiments in Granular HMX," in *JANNAF Propulsion Systems Hazards Subcommittee Meeting*, Palm Beach, FL, 1997.

[31] S. Mallat, A Wavelet Tour of Signal Processing, San Diego, CA: Academic Press, 1999.

[32] A. Grossmann and J. Morlet, "Decomposition of Functions into Wavelets of Constant Shape, and Related Transforms," University of Bielefeld, France, 1984.

[33] J. C. Hong and Y. Y. Kim, "Determination of the Optimal Gabor Wavelet Shape for the Best Time-Frequency Localization Using the Entropy Concept," *Experimental Mechanics,* vol. 44, no. 4, pp. 387-395, 2004.

[34] N. Delprat, B. Escudie, P. Guillemain, R. Kronland-Martinet, P. Tchamitchian and B. Torresani, "Asymptotic Wavelet and Gabor Analysis: Extraction of Instantaneous Frequencies," *IEEE Transactions on Informational Theory,* vol. 38, no. 2, pp. 644-664, 1992.

[35] I. Simonovski and M. Boltezar, "The Norms and Variances of the Gabor, Morlet and General Harmonic Wavelet Functions," *Journal of Sound and Vibration,* vol. 264, pp. 545-557, 2003.

[36] M. Boltezar and J. Slavic, "Enhancements to the Continuous Wavelet Transform for Damping Identifications on Short Signals," *Mechanical Systems and Signal Processing,* vol. 18, pp. 1065-1076, 2004.

[37] J. Slavic, M. Simonovski and M. Boltezar, "Damping Identification Using a Continuous Wavlet Transform Application to Real Data," *Journal of Sound and Vibration,* vol. 262, no. 2, pp. 291-307, 2003.

[38] D. E. Kittell and J. O. Mares, "Measuring Time-Resolved Detonation Velocity Using Wavelet Analysis and Microwave Interferometry," *Review of Scientific Instruments [to be submitted],* 2014.

[39] A. Savitzky and M. J. Golay, "Smoothing and Differentiation of Data by Simplified Least Squares Procedures," *Analytical Chemistry,* vol. 36, no. 8, pp. 1627-1639, 1964.

[40] L. D. Landau and E. M. Lifshitz, Electrodynamics of Continuous Media, vol. Volume 8 of Course of Theoretical Physics, New York: Pergamon Press, 1960.

[41] H. Looyenga, "Dielectric Constants of Heterogeneous Mixtures," *Physica,* vol. 31, pp. 401-406, 1965.

[42] D. C. Dube, "Study of Landau-Lifshitz-Looyenga's Formula for Dielectric Correlation Between Powder and Bulk," *J. Phys. D: Appl. Phys,* vol. 3, pp. 1648-1652, 1970.

[43] Los Alamos Scientific Laboratory, LASL Explosive Property Data, T. R. Gibbs and A. Popolato, Eds., Berkeley, California: University of California Press, 1980.

[44] L. Fried and P. Souers, "CHEETAH: A Next Generation Thermochemical Code," Lawerance Livermore Natonal Laboratory Report #UCRL-ID-117240, Livermore, 1994.

[45] J. M. Majowicz and S. J. Jacobs, "Initiation to Detonation of High Explosives by Shocks," U.S. Naval Ordnance Laboratory, White Oak, Maryland, 1958.

[46] A. W. Campbell, W. C. Davis, J. B. Ramsay and J. R. Travis, "Shock Initiation of Solid Explosives," *The Physics of Fluids,* vol. 4, no. 4, pp. 511-521, 1961.

[47] P. W. Cooper, Explosives Engineering, New York: Wiley-VCH, 1996.

[48] J. B. Ramsay and A. Popolato, "Analysis of Shock Wave Initiation Data for Solid Explosives," in *Fourth Symposium (International) on Detonation*, White Oak, Maryland, 1965.